RSC Advances

PAPER

Check for updates

Solution-processed inorganic copper(I) thiocyanate as a hole injection layer for high-performance quantum dot-based light-emitting diodes

Tao Ding,[a] Ning Wang,[a] Chen Wang,[b] Xinghua Wu,[b] Wenbo Liu,[a] Qichun Zhang, [ID][b] Weijun Fan[a] and Xiao Wei Sun*[c]

We report the advantageous properties of inorganic copper(I) thiocyanate (CuSCN) as a solution-processable hole injection material in quantum dot-based light-emitting diodes (QLEDs). CuSCN, with its high work function, it decreases the turn-on voltage (V_{th}) by 0.8 volt to 3.4 V as compared with devices based on the most-widely used poly(3,4-ethylenedioxythiophene):poly(styrenesulfonate) (PEDOT:PSS) ($V_{th} = 4.2$ V). As a transparent, highly stable and low cost commercial material, CuSCN acting as the hole injection layer (HIL) gives the QLED better V_{th}, and comparable performance to PEDOT:PSS-based QLED for other parameters including maximum luminance and external quantum efficiency. The decreased V_{th} can improve the power efficiency and is a necessary step in meeting market demand. The successful demonstration of the solution-processed inorganic HIL using simple and low temperature processing routes provide guidelines and prospects for the development of reliable all-inorganic and tandem QLEDs and possible commercial applications at a large scale.

In 1994, A. P. Alivisatos and his colleagues incorporated cadmium selenide (CdSe) quantum dots (QDs) into light-emitting devices (LEDs) and reported an external quantum efficiency (EQE) of 0.001–0.01% for the first time.[1] Since then, quantum dot-based light-emitting diodes (QLEDs) have received considerable attention due to their extraordinary properties including high photoluminescence quantum yield (PL QY), tunable narrow-band emission over the whole visible spectrum, simple colloidal synthetic processes and solution processability.[2–5] Recently, we have witnessed significant achievements in both the design and optimization of both QDs and QLEDs. In 2013, Mashford et al. reported red QLEDs with the maximum EQE of 18%, which is close to the theoretical maximum of 20% and more importantly, comparable with the performance of the state-of-the-art organic LED (OLED) technology.[4] The performance of red QLED was further improved by X. G. Peng et al. in 2014.[6] They reported high-performance, all-solution-processed red QLED with the key parameters including EQE, turn-on voltage (V_{th}), color purity, etc. that are superior or at least comparable with these of other high-performance red LEDs. Furthermore, by preciously tuning the composition of

QDs, P. H. Holloway and L. Qian et al. successfully presented a full series of blue, green and red QLEDs with low V_{th}, saturated colors and high EQEs (all over 10%).[7]

To date, much of such progress have been made in the normal architecture consisting of multiple layers where the active layer is sandwiched by bottom hole injection/transporting layer (HIL/HTL) and top electron transport layer (ETL), while these layers are normally spin-coated sequentially from orthogonal solvents.[3,6–11] For the ideal HIL/HTL materials, following requirements should be met: (1) high transparency across the full visible spectrum;[12,13] (2) suitable energy level for efficient hole injection and electron blocking from active QD layer;[11,14,15] (3) accessible deposition technique and following post-processing conditions.[12,13,16–20] In term of these, poly(3,4-ethylenedioxythiophene):poly(styrenesulfonate) (PEDOT:PSS) has been regarded as the most universal HIL/HTL not only in QLED but also in OLED and organic photovoltaic (OPV) devices because of its superior transparency, smooth surface over large areas, good conductivity and moderate work function.[2,21–23] Despite these advantages and certified applications in opto-electronic devices, however, PEDOT:PSS itself has certain limitations. The acidic and hygroscopic nature as well as the thermal instability will influence the device performance and result in degradation.[24] Moreover, due to its semi-metallic nature, PEDOT:PSS cannot be qualified as a good electron blocking layer.[25] A better HIL is needed for QLED.

In order to address the issues of PEDOT:PSS, an alternative approach is to use inorganic metal oxides, such as nickel oxide

[a]School of Electrical and Electronic Engineering, Nanyang Technological University, 50 Nanyang Avenue, Singapore 639798

[b]School of Materials Science and Engineering, Nanyang Technological University, 50 Nanyang Avenue, Singapore 639798

[c]Department of Electrical and Electronic Engineering, Southern University of Science and Technology, 1088 Xueyuan Road, Nanshan, Shenzhen, Guangdong 518055, China. E-mail: sunxw@sustc.edu.cn

(NiO), vanadium oxide (V$_2$O$_5$), tungsten oxide (WO$_3$), copper oxide (CuO), or molybdenum oxide (MoO$_3$) as the HIL/HTL.[11,14,26–28] These layers can be deposited by either radio-frequency sputtering,[29] thermal evaporation under high vacuum[30] or by solution process based on either the decomposition of organic–inorganic hybrid precursors or the annealing of nanoparticle suspensions.[14,26] Sputtering technique has been demonstrated to result in low efficiency due to the generated rough interface between the sputtered NiO and ITO electrode, while thermal evaporation is relatively more costly and wasteful in terms of raw materials. Therefore, solution-processed inorganic semiconductor films have received more and more attentions. Our group has successfully reported using WO$_3$ and CuO as hole injection materials for efficient QLEDs, demonstrating comparable device performance compared to PEDOT:PSS-based QLED.[14,28] However, the metal oxide film normally needs high-temperature annealing to acquire suitable transparency and conductivity;[31] some of the metal oxide films require extra O$_2$-plasma treatment to remove the polymeric dispersing agent for better hole injection; such requirements are contradictory for the initial purpose of applying inorganic materials as a replacement for PEDOT:PSS.

Here, for the first time we reported the utilization of solution-processed copper thiocyanate (CuSCN) film as the hole injection layer for QLED. With its high transparency across the whole visible spectrum and intrinsic p-type conductivity, CuSCN, which is available at low cost and can be directly solution processed or doctor blading by dissolving in suitable solvents, has been demonstrated as a qualified HTL/HIL in transistors,[13] perovskite solar cells,[16,20,32] organic/QD photovoltaic cells[12,17,19,33] and OLEDs.[34] Moreover, there is a unique highlight of using CuSCN as the HIL in QLED. It has been well recognized that in QLEDs with normal structure, electrons are injected spontaneously from cathode while holes encounter barriers during the injection process because of the deep valance band energy of QDs, resulting in an unbalanced charge injection.[6] Compared with PEDOT:PSS, CuSCN has a high hole mobility of 0.01–0.1 cm^2 V^{-1} s^{-1} and a deeper valance band maximum (VBM) around 5.5 eV,[13,16,35,36] therefore hole injection in QLED is more efficient and consequently, improved device performance can be further expected.

Fig. 1a shows the schematic device configuration of QLED, and consists of multiple layers of, in the following order,

indium tin oxide (ITO), a PEDOT:PSS or CuSCN HIL (40 nm), poly(9-vinlycarbazole) (PVK, 40 nm), CdSe@ZnS core–shell QDs (40 nm), 2,2′,2′′-(1,3,5-benzinetriyl)-tris(1-phenyl-1H-benzimidazole) (TPBi, 35 nm), lithium fluoride (LiF, 1 nm) and aluminum (Al, 100 nm). The relative energy level positions of the materials used in QLED are shown in Fig. 1b, with these values taken from reported literatures.[9,12,14] The valance band maximum (VBM) of CuSCN is around 5.5 eV, which is deeper than the highest occupied molecular orbital (HOMO) level of PEDOT:PSS. As can be expected, such difference is supposed to have a profound effect on device performance.

It is necessary to compare the structural and optical properties for CuSCN and PEDOT:PSS. Fig. 2a–c show the atomic force microscopy (AFM) topographic images for ITO, ITO/PEDOT:PSS and ITO/CuSCN deposited onto the glass substrates, respectively. The RMS surface roughness of pure ITO film has a value of 0.98 nm. After spin-coating PEDOT:PSS on top if the ITO substrate, the surface roughness was slightly increased to a RMS value of 1.97 nm with a smooth morphology. On the other hand, for the ITO substrate coated with CuSCN HIL, the RMS roughness increases 4.75 nm; these values are in good correspondence with the reported ones.[19] The AFM measurements demonstrate the successful CuSCN film formation onto the ITO/glass substrates by solution process although further optimization is still needed.

The X-ray diffraction (XRD) analysis was conducted to investigate the crystallinity of CuSCN film. Fig. 3a shows the diffraction pattern of the CuSCN film spin-coated from DES solutions, demonstrating an amorphous characteristic with no diffraction peaks. Since the device described in this work has a bottom-anode, bottom-emitting LED architecture, it is important to compare the optical transmittance of different HIL materials used, which makes the optical transparency measurement necessary. Fig. 3b shows the absorption spectra (in the visible range of 350–700 nm) of glass substrates with PEDOT:PSS and CuSCN with the same thickness deposited directly on top. The result shows that CuSCN exhibits high transparency in the wavelength above 500 nm and a slight increasing absorption in the short wavelength region due to its wide optical bandgap (>3.5 eV).[13,19] On the other hand, PEDOT:PSS tends to have less absorption in the short-wavelength region but absorbs more beyond 550 nm to the red region. Such optical characteristic of PEDOT:PSS should be
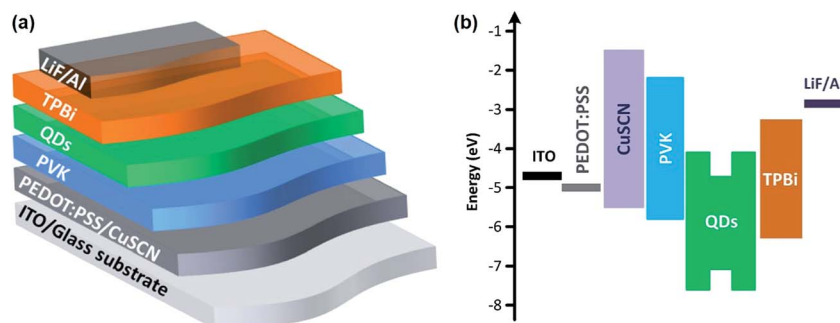

Fig. 1 (a) Schematic of layers in the device structure and (b) flat–band energy level diagram of materials used in QLEDs.
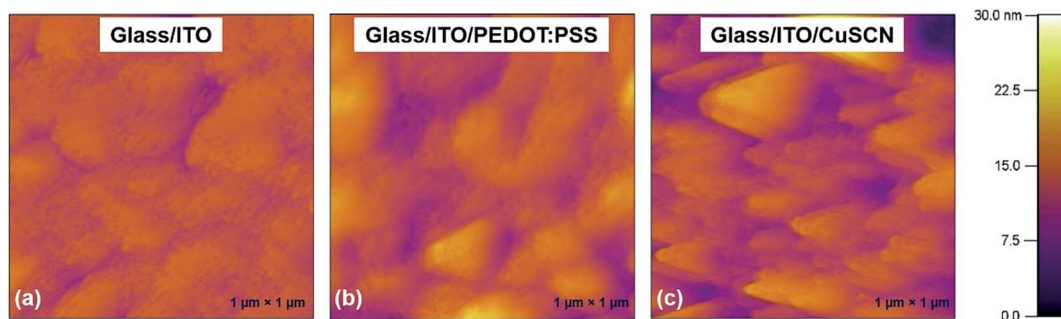
Fig. 2 AFM topography images of (a) ITO, (b) PEDOT:PSS and (c) CuSCN films deposited onto glass substrates, respectively.
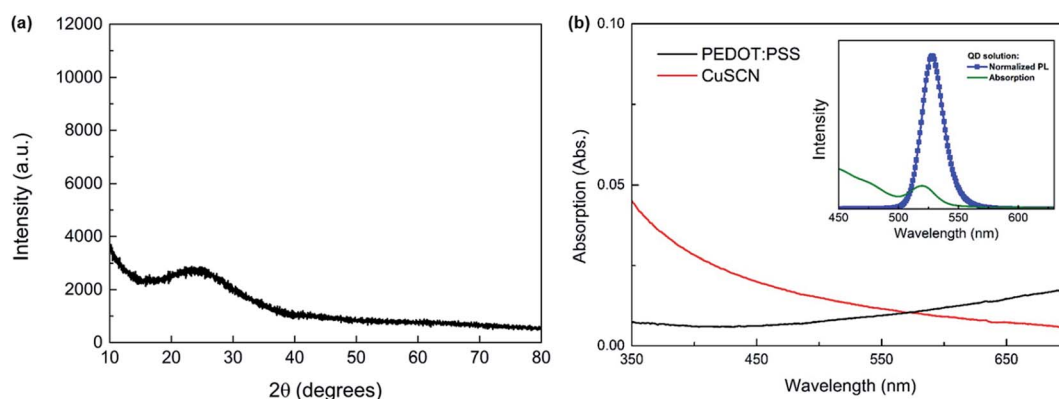

Fig. 3 (a) X-ray diffraction pattern of the CuSCN film dissolved in DES; (b) absorption spectra of PEDOT:PSS and CuSCN films spin-coated on glass substrates with the same thickness (45 nm). Inset: ultraviolet-visible absorption and photoluminescence spectra of QD solutions.

attributed to the intragap absorptions originated from the polaronic changes due to the introduced oxidative doping for better conductivity purpose.[34]

To further confirm the usefulness of CuSCN film in QLEDs, two sets of devices with PEDOT:PSS/CuSCN as HILs were fabricated with a spin-coated green-emitting QD film as the active layer. The inset of Fig. 3 shows the photoluminescence (excited by 325 nm source) and the ultraviolet-visible absorption spectra of QD solutions (dissolved in toluene). Further the PL spectrum of QD was compared with the normalized electroluminescence (EL) spectra of the QLEDs based on CuSCN and PEDOT:PSS HILs acquired at an applied voltage of 5 V, as shown in Fig. 4a, respectively. It can be distinctly observed that both the PL spectrum of QD solution and the EL spectra of QLEDs are identical, showing a Gaussian shape emission curve with center wavelength at 528 nm and a full-width at half-maximum (FWHM) of 20 nm. Fig. 4b gives the EL spectra evolution of CuSCN-based device under different applied voltages, demonstrating that the EL spectra shapes under increasing voltages are identical to the PL emission of QD solution. The perfectly overlapped EL spectra from devices with the voltage-dependent EL spectra evolution of CuSCN-based device together demonstrate not only a stable recombination zone under increasing applied voltages but also the efficient hole injection capabilities of CuSCN.

Fig. 4c shows the current density–voltage–luminance (J–V–L) characteristics for CuSCN and PEDOT:PSS-based QLEDs,

respectively. The workfunction of PEDOT:PSS has a reported value of 4.9–5.2 eV;[6,14] compared with the HOMO level of PVK (5.8 eV), there exists an energy barrier of 0.6–0.9 eV, which is unfavorable for hole injection in PEDOT:PSS-based QLED. Such a noteworthy barrier can be reflected by the high turn-on voltage with a value of 4.2 V (to reach a luminance of 1 cd m^{-2}); on the other hand, the turn-on voltage of CuSCN-based QLED decreases by 0.8 volt to 3.4 V. This decreased turn-on voltage should be related to the reduced energy barrier for hole injection resulting from the deeper VBM of CuSCN (5.5 eV), which is in good agreement with our expectation and other reports as well.[13] Fig. 4d and e show a comparison of the external quantum efficiency–current density (EQE–J) and current efficiency–current density (CE–J) characteristics of the CuSCN-based and an optimized PEDOT:PSS-based QLEDs with the same device configuration, respectively. To be specific, our best performing QLED based on CuSCN yields maximum luminance of 140 000 cd m^{-2}, maximum current efficiency of 28.4 cd A^{-1} with an EQE of 6.9%. The key figures of QLEDs based on PEDOT:PSS as HIL are also given in Table 1 for comparison.

As already highlighted, one of the key benefits regarding the use of CuSCN as HIL is its improved capability of injecting holes in QLED due to its deeper hole injection level as well as high hole mobility.[19] To demonstrate this further, we prepared two sets of hole-only devices with a multilayer structure of ITO/HIL/PVK (40 nm)/QDs (40 nm)/Au (100 nm), one with CuSCN and the other with PEDOT:PSS as the HIL while the other layers are
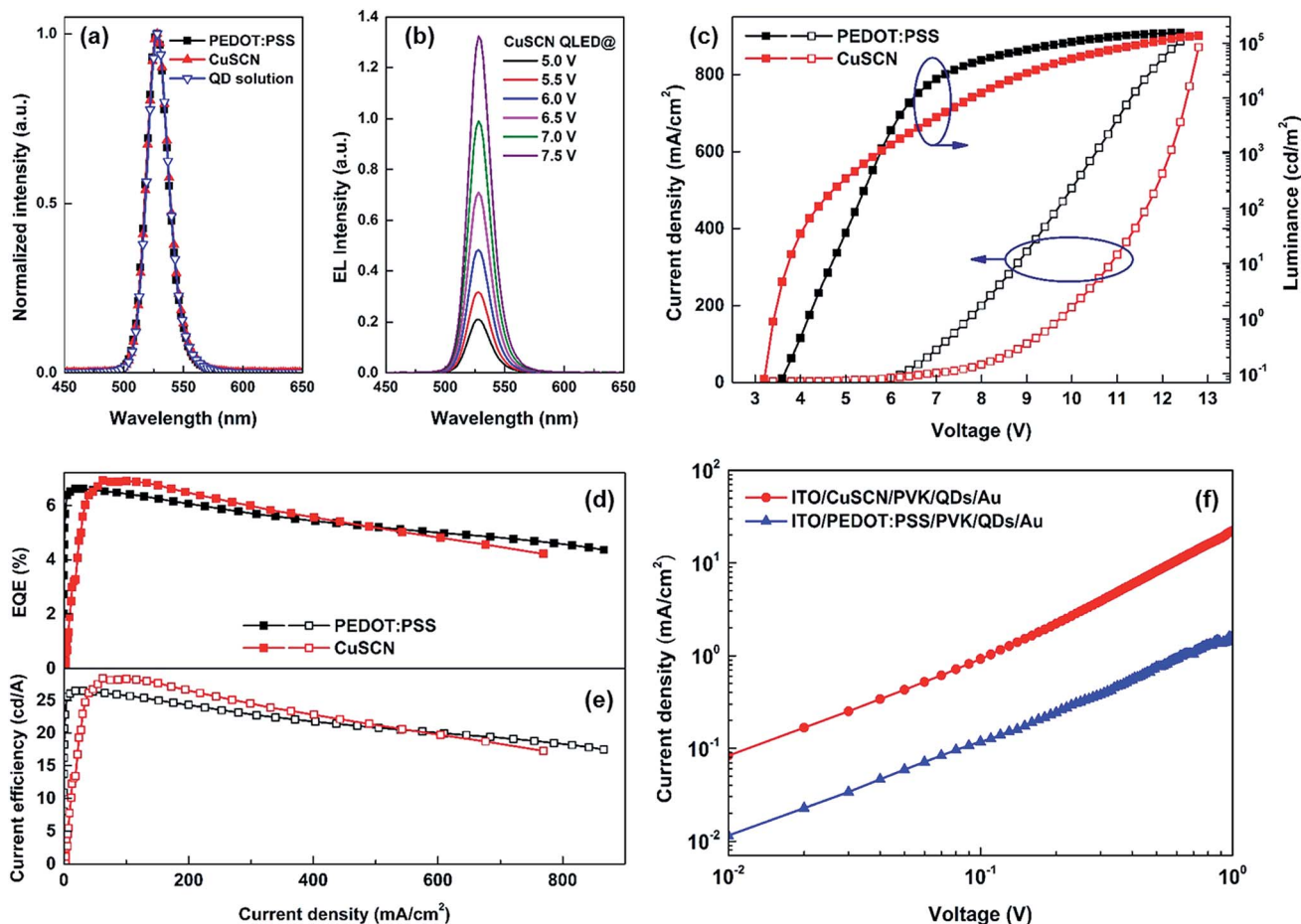
Fig. 4 Comparison of device performance for CuSCN and PEDOT:PSS HIL QLEDs. (a) Normalized EL spectra of QLEDs based on CuSCN and PEDOT:PSS HIL compared with QD PL spectra; (b) EL spectrum evolution under different applied voltages for CuSCN-based QLEDs; (c) current density–voltage–luminance (J–V–L) characteristics for CuSCN and PEDOT:PSS-based QLEDs; (d) external quantum efficiency (EQE) of CuSCN and PEDOT:PSS-based QLEDs as a function of current density; (e) current efficiency (CE) *versus* current density characteristics for both devices; (f) electrical measurements on the current density–voltage curves for the hole only devices based on CuSCN and PEDOT:PSS, respectively.

Table 1 Comparison of parameters of device performance using CuSCN and PEDOT:PSS as HILs, respectively

Type of HIL	Turn-on voltage [V]@1 cd m^{-2}	Max. luminance [cd m^{-2}]	Max. current efficiency [cd A^{-1}]	Max. EQE [%]
PEDOT:PSS	4.2	151 400	26.5	6.6
CuSCN	3.4	146 700	28.4	6.9

identical. Fig. 4f gives the comparison of current density–voltage characteristics of both hole-only devices, clearly demonstrating that the current density of CuSCN-based hole-only device is almost one order of magnitude greater than that of the PEDOT:PSS-based ones. It should be noted that in such hole-only devices, the current will only represent the behavior of hole transportation because the electrons are blocked by the PVK layer; since there are no difference in these two hole-only devices except the HIL, it is safe to attribute the improved hole current to the introduction of CuSCN as a replacement for PEDOT:PSS.

In conclusion, we reported the successful application of a solution-processed CuSCN film as the hole injection layer for high performance QLEDs. Due to its optical transparency, desirable energy level and high hole mobility, CuSCN reduces the turn-on voltage of QLED by 0.8 volt while achieving better or at least comparable performance relative to control device based on PEDOT:PSS. The resulted device presents a maximum luminance exceeding 140 000 cd m^{-2} with best current efficiency over 28 cd A^{-1}. Such performance is attributed to effective hole injection, reduced energy barrier and better charge balance resulted from CuSCN. To the best of our knowledge, this work is the first attempt using this material as the efficient

hole injection layer in QLED. As a relatively cheap material, we believe CuSCN can further act as an ideal inorganic hole injection candidate for all-inorganic or tandem QLEDs fabrication with further optimization.

Experimental section

Preparation of CdSe@ZnS QDs and CuSCN solution

The CdSe@ZnS core–shell quantum dots (QDs) were synthesized according to the previously reported procedure with some modifications.[9,37] Briefly, 0.14 mmol of cadmium acetate (0.14 mmol), zinc oxide (3.41 mmol) and oleic acid (OA, 7 ml) were mixed in a 100 ml four-neck flask and heated to 100 °C with degassing for 20 min. Then, 1-octadecene (1-ODE, 15 ml) was injected into the reactor, and the whole mixture was further degassed and heated. After, the reactor was filled with argon and swiftly heated to 310 °C. Then, 2 ml of trioctylphosphine (TOP) containing selenium (Se, 2 mmol) and sulfur (S, 2 mmol) was swiftly injected into the hot mixture and maintaining for 10 min. In order to coat an additional ZnS shell, 1-ODE (2.4 ml) containing 1.6 mmol S was injected and the mixture was left to react for 12 min. Then 9.5 ml $Zn(OA)_2$ was injected and the temperature was controlled to 270 °C. Next, TOP 9.65 mmol of S dissolved in TOP (5 ml) was injected into the mixture at a rate of 10 ml min^{-1}. The reaction was maintained at that temperature for 20 min for outmost shell formation. The QDs were purified by acetone and methanol and re-dispersed in toluene for later use. For CuSCN (Sigma-Aldrich), the as-received powder was dissolved in diethyl sulfide (DES, Sigma-Aldrich) with a concentration of 20 mg ml^{-1} with overnight stirring.

Device fabrication and characterization

Glass substrates with patterned ITO are sonicated by ITO detergent, de-ionized water, acetone and isopropyl alcohol sequentially. First, a HIL was deposited on top. For PEDOT:PSS (Clevios P VP Al 4083), the solution was filtered by 0.45 µm PVDF filter and then spin-coated onto ITO at 4000 rpm for 60 s, baking at 150 °C for 30 min. For CuSCN HIL, the desired film was acquired under a speed of 2000 rpm for 60 s with annealing temperature of 120 °C for 20 min. PVK (10 mg ml^{-1} dissolved in chlorobenzene) and QD solutions (10 mg ml^{-1} in toluene) were spin-coated with optimized speeds and annealing temperatures. Then, on top of QD layer, TPBi, LiF and aluminum were thermally evaporated in sequence under a base pressure of ~1.0 × 10^{-6} torr. The effective area of QLED is 2 × 2 mm^2 defined by the overlapped area of ITO and Al electrodes. Surface roughness measurement was performed by using AFM (Cypher S, Asylum Research) for film imaging. The XRD measurement was performed by Shimadzu XRD-6000 with Cu-Kα radiation operated at 40 kV and 30 mA and a scintillation counter scintillator as detector. A Shimadzu RF-5301PC spectrofluorophotometer and a Shimadzu UV-1800 spectrophotometer were used to obtain the photoluminescence and absorption spectra of QD solutions, respectively. The current density–luminance–voltage (J–L–V) characteristics and the electroluminescence spectra were acquired simultaneously by using a programmable Yogakawa GS610 source measurement unit with a spectrometer (PhotoResearch SpectraScan PR 705). All measurements were carried out at room temperature under ambient conditions without encapsulation.

Acknowledgements

References

1 V. Colvin, M. Schlamp and A. Alivisatos, *Nature*, 1994, **370**(6488), 354–357.

2 Q. Sun, Y. A. Wang, L. S. Li, D. Wang, T. Zhu, J. Xu, C. Yang and Y. Li, *Nat. Photonics*, 2007, **1**(12), 717–722.

3 L. Qian, Y. Zheng, J. Xue and P. H. Holloway, *Nat. Photonics*, 2011, **5**(9), 543–548.

4 B. S. Mashford, M. Stevenson, Z. Popovic, C. Hamilton, Z. Q. Zhou, C. Breen, J. Steckel, V. Bulovic, M. Bawendi, S. Coe-Sullivan and P. T. Kazlas, *Nat. Photonics*, 2013, **7**(5), 407–412.

5 T. Ding, X. Y. Yang, L. Ke, Y. J. Liu, W. Y. Tan, N. Wang, X. H. Zhu and X. W. Sun, *Org. Electron.*, 2016, **32**, 89–93.

6 X. Dai, Z. Zhang, Y. Jin, Y. Niu, H. Cao, X. Liang, L. Chen, J. Wang and X. Peng, *Nature*, 2014, **515**(7525), 96–99.

7 Y. X. Yang, Y. Zheng, W. R. Cao, A. Titov, J. Hyvonen, J. R. Manders, J. G. Xue, P. H. Holloway and L. Qian, *Nat. Photonics*, 2015, **9**(4), 259–266.

8 K.-H. Lee, J.-H. Lee, W.-S. Song, H. Ko, C. Lee, J.-H. Lee and H. Yang, *ACS Nano*, 2013, **7**(8), 7295–7302.

9 K. H. Lee, J. H. Lee, H. D. Kang, B. Park, Y. Kwon, H. Ko, C. Lee, J. Lee and H. Yang, *ACS Nano*, 2014, **8**(5), 4893–4901.

10 H. Shen, W. Cao, N. T. Shewmon, C. Yang, L. S. Li and J. Xue, *Nano Lett.*, 2015, **15**(2), 1211–1216.

11 X. Yang, Y. Ma, E. Mutlugun, Y. Zhao, K. S. Leck, S. T. Tan, H. V. Demir, Q. Zhang, H. Du and X. W. Sun, *ACS Appl. Mater. Interfaces*, 2013, **6**(1), 495–499.

12 N. D. Treat, N. Yaacobi-Gross, H. Faber, A. K. Perumal, D. D. C. Bradley, N. Stingelin and T. D. Anthopoulos, *Appl. Phys. Lett.*, 2015, **107**(1), 013301.

13 P. Pattanasattayavong, N. Yaacobi-Gross, K. Zhao, G. O. N. Ndjawa, J. Li, F. Yan, B. C. O'Regan, A. Amassian and T. D. Anthopoulos, *Adv. Mater.*, 2013, **25**(10), 1504–1509.

14 T. Ding, X. Y. Yang, L. Y. Bai, Y. B. Zhao, K. E. Fong, N. Wang, H. V. Demir and X. W. Sun, *Org. Electron.*, 2015, **26**, 245–250.

15 V. Wood, M. Panzer, J. Halpert, J.-M. Caruge, M. Bawendi and V. Bulovic, *ACS Nano*, 2009, **3**(11), 3581–3586.

16 P. Qin, S. Tanaka, S. Ito, N. Tetreault, K. Manabe, H. Nishino, M. K. Nazeeruddin and M. Gratzel, *Nat. Commun.*, 2014, **5**, 3834.

17 N. Chaudhary, R. Chaudhary, J. P. Kesari, A. Patra and S. Chand, *J. Mater. Chem. C*, 2015, **3**(45), 11886–11892.

18 N. Wijeyasinghe and T. D. Anthopoulos, *Semicond. Sci. Technol.*, 2015, **30**(10), 104002.

19 N. Yaacobi-Gross, N. D. Treat, P. Pattanasattayavong, H. Faber, A. K. Perumal, N. Stingelin, D. D. C. Bradley, P. N. Stavrinou, M. Heeney and T. D. Anthopoulos, *Adv. Energy Mater.*, 2015, **5**(3), 1401529.

20 S. Ye, W. Sun, Y. Li, W. Yan, H. Peng, Z. Bian, Z. Liu and C. Huang, *Nano Lett.*, 2015, **15**(6), 3723–3728.

21 N. Wang, Z. Chen, W. Wei and Z. Jiang, *J. Am. Chem. Soc.*, 2013, **135**(45), 17060–17068.

22 R. Hikmet, D. Talapin and H. Weller, *J. Appl. Phys.*, 2003, **93**(6), 3509–3514.

23 Y. Zhao, J. Chen and D. Ma, *ACS Appl. Mater. Interfaces*, 2013, **5**(3), 965–971.

24 J.-M. Caruge, J. E. Halpert, V. Bulovic and M. G. Bawendi, *Nano Lett.*, 2006, **6**(12), 2991–2994.

25 D. Poplavskyy, J. Nelson and D. Bradley, *Appl. Phys. Lett.*, 2003, **83**(4), 707–709.

26 J. R. Manders, S. W. Tsang, M. J. Hartel, T. H. Lai, S. Chen, C. M. Amb, J. R. Reynolds and F. So, *Adv. Funct. Mater.*, 2013, **23**(23), 2993–3001.

27 J. You, L. Meng, T.-B. Song, T.-F. Guo, Y. M. Yang, W.-H. Chang, Z. Hong, H. Chen, H. Zhou and Q. Chen, *Nat. Nanotechnol.*, 2016, **11**(1), 75–81.

28 X. Yang, E. Mutlugun, Y. Zhao, Y. Gao, K. S. Leck, Y. Ma, L. Ke, S. T. Tan, H. V. Demir and X. W. Sun, *Small*, 2014, **10**(2), 247–252.

29 J. Caruge, J. Halpert, V. Wood, V. Bulović and M. Bawendi, *Nat. Photonics*, 2008, **2**(4), 247–250.

30 X. Yang, P. L. Hernandez-Martinez, C. Dang, E. Mutlugun, K. Zhang, H. V. Demir and X. W. Sun, *Adv. Opt. Mater.*, 2015, 1439–1445.

31 M. T. Greiner and Z.-H. Lu, *NPG Asia Mater.*, 2013, **5**(7), e55.

32 K. Zhao, R. Munir, B. Yan, Y. Yang, T. Kim and A. Amassian, *J. Mater. Chem. A*, 2015, **3**(41), 20554–20559.

33 N. R. Paudel and Y. F. Yan, *Prog. Photovoltaics*, 2016, **24**(1), 94–101.

34 A. Perumal, H. Faber, N. Yaacobi-Gross, P. Pattanasattayavong, C. Burgess, S. Jha, M. A. McLachlan, P. N. Stavrinou, T. D. Anthopoulos and D. D. Bradley, *Adv. Mater.*, 2015, **27**(1), 93–100.

35 P. Pattanasattayavong, G. O. N. Ndjawa, K. Zhao, K. W. Chou, N. Yaacobi-Gross, B. C. O'Regan, A. Amassian and T. D. Anthopoulos, *Chem. Commun.*, 2013, **49**(39), 4154–4156.

36 P. Pattanasattayavong, V. Promarak and T. D. Anthopoulos, *Adv. Electron. Mater.*, 2017, **3**(3), 1600378.

37 W. K. Bae, K. Char, H. Hur and S. Lee, *Chem. Mater.*, 2008, **20**(2), 531–539.